Journal of Thermal Analysis and Calorimetry (2022) 147:9291–9299
https://doi.org/10.1007/s10973-021-11173-8

Volatility of sodium, potassium, and cesium perrhenates determined by thermogravimetry

Pornsinee Cholsaipant[1] · Jaime L. George[1] · Dongsang Kim[1] · Albert A. Kruger[2]

Received: 24 May 2021 / Accepted: 1 December 2021 / Published online: 15 February 2022

Abstract

In this study, we investigated the volatility of sodium, potassium, and cesium perrhenates using thermogravimetry (TG) performed on single salts and their binary mixed salts. We performed simultaneous TG and differential scanning calorimetry under a ramp heating condition at 10 °C/min up to 1200 °C to characterize volatilization behavior as a function of temperature. We also performed isothermal TG over a temperature range of 700–975 °C. To estimate the relative differences in the vapor pressure of the alkali perrhenates we adopted a published equation on the vaporization mass loss rate during diffusion-controlled evaporation, applied a proposed equation on the interdiffusion coefficient of vapors, and used the literature data available on vapor pressure for $KReO_4$. Both the temperature ranges of evaporation determined by TG under ramp heating conditions and the vapor pressure estimated from isothermal TG support that the order of volatility of alkali perrhenates is $CsReO_4 > KReO_4 > NaReO_4$. This result does not support the unusual volatility order of $KReO_4 > CsReO_4 > NaReO_4$ observed from Hanford LAW glass feeds, which suggests that the volatility of the perrhenates is likely dependent on the composition of salt in which the perrhenates are dissolved.

Keywords Thermal analysis · Alkali perrhenate · Technetium · Rhenium · Volatilization

Introduction

Decades-long plutonium production and reprocessing operations at the U.S. Department of Energy's Hanford Site in southeastern Washington state generated approximately 200 million liters of chemical and radioactive wastes that currently are stored in underground tanks [1, 2]. The removal and treatment of this waste falls under the jurisdiction of the Department of Energy, Office of River Protection. To facilitate treatment, the waste will be separated into a low-activity waste (LAW) fraction and a high-level waste (HLW) fraction, each of which has different methods and constraints surrounding its processing. Part of the LAW portion will be treated in advance of completion of the whole plant, through the Direct-Feed, Low-Activity Waste (DFLAW) process which will use the Hanford Site's Waste Treatment and Immobilization Plant (WTP) Low-Activity Waste Facility, the Analytical Laboratory and the supporting facilities that run the plant [3]. These LAWs are composed of mostly sodium nitrate, nitrite, aluminate, phosphate, and sulfate, with various numbers of minor and trace metals, organics, and radionuclides. Glass-making additives will be added to the liquid waste to form slurries that will be fed to a glass melter to vitrify the LAW into glass waste forms for final disposal [4].

One of the radionuclides that poses a great challenge in nuclear waste remediation is technetium-99 (^{99}Tc or Tc-99). The primary form of Tc-99 in Hanford tank waste is the water soluble pertechnetate (TcO_4^-) ion [5]. The baseline flowsheet for the WTP dictates that Tc-99 will not be removed from the aqueous waste fraction, leaving the majority of Tc-99 in the LAW stream. Although the concentration of Tc-99 present in the aqueous LAW

✉ Dongsang Kim
dongsang.kim@pnnl.gov

Pornsinee Cholsaipant
peyton0394@gmail.com

Jaime L. George
jaime.george@pnnl.gov

Albert A. Kruger
albert_a_kruger@orp.doe.gov

[1] Present Address: Pacific Northwest National Laboratory, Richland, WA 99352, USA

[2] U.S. Department of Energy, Office of River Protection, Richland, WA 99352, USA

is relatively low (~ 0.05 mM on average) [3] compared to other major constituents, its long half-life and high mobility in groundwater makes it a major risk contributor to the integrated disposal facility performance assessment [6]. In addition to creating challenges for the long-term disposal of nuclear waste, the high volatility of Tc-99 at elevated temperatures under aerobic conditions also significantly challenges the vitrification process [7].

Previous studies have used rhenium (Re) as a non-radioactive surrogate to study the incorporation behavior of Tc-99 into waste glass because of its similar chemical affinity and volatilization behavior during vitrification [5, 8]. Depending on the melter feed composition and operating parameters, studies have shown that the amount of Tc-99 and Re retained in glass varies greatly from 18 to 66% [9, 10]. One of the current strategies to maximize the final retention of Tc-99 in the glass waste form includes collecting and recycling the Tc-containing off-gas stream to the melter. The down side of this approach is that in addition to collecting the volatilized Tc-99, it also collects other volatile components such as sulfur and chlorine that are known to limit waste loading in glass [4]. Therefore, understanding Tc-99 volatilization mechanisms during the feed-to-glass conversion process is important in the development of technologies to increase the final Tc-99 retention and optimize the waste treatment and disposal processes at the Hanford Site.

One of the long-standing questions related to the volatilization of Tc-99 and Re during vitrification of wastes was the form of Tc-99 and Re that volatilize. Kim and Kruger [7] reviewed published data ranging from evaporation of simple and mixed salts to volatilization of Re and Tc-99 during melting of various simulated waste glasses. They strongly argued that, although there was no direct evidence, Tc and Re volatilize as alkali pertechnetate and alkali perrhenate without decomposition (e.g., $2KReO_4 \rightarrow K_2O + Re_2O_7$) during melting of Hanford waste glass feeds. One of the interesting findings reported in Kim and Kruger's review [7] was some data suggest that the volatility of alkali perrhenates during melting of simulated Hanford LAW glass feeds is in the order of $KReO_4 > CsReO_4 > NaReO_4$, which is contrary to a general trend that the properties of alkali compounds follow the atomic number of alkali metals. Thermodynamic properties of some single and mixed salts of alkali perrhenates have been studied [11–18], but volatility data in the literature is scarce except for information about $KReO_4$ that was reported by Lebedev [19]. As a first step to understanding the volatile behavior of Re as alkali perrhenate during simulated LAW glass melting, we studied the melting characteristics and volatilization behavior of three alkali perrhenates and their binary mixed salts using TG under both ramp heating and isothermal heating conditions.

Materials and experimental procedure

Alkali perrhenate salts of $NaReO_4$ (Alfa Aesar; lot# X210B10), $KReO_4$ (Alfa Aesar; lot# A30P09), and $CsReO_4$ (American Elements; lot# 1,192,026,347–401) with ≥ 99% purity were used. Binary salt mixtures—$NaReO_4$–$CsReO_4$, $NaReO_4$–$KReO_4$, and $KReO_4$–$CsReO_4$—were prepared at a 1:1 molar ratio in ~ 1 g quantity. Each salt was weighed to the nearest 0.1 mg and the mixtures were combined with an agate mortar and pestle. Aliquots of this 1 g mixture then were used for thermal analysis measurements. All mass measurements were done with a Mettler Toledo XPE 205 Delta Range scale.

Thermogravimetry–differential scanning calorimetry (TG-DSC) measurements were made under both ramp heating and isothermal conditions for all single alkali perrhenate salts and binary perrhenate salt mixtures. Ramp heating TG-DSC measurements were taken with an STA 499 F1 Jupiter TG-DSC manufactured by NETZSCH. In each experiment, an ~ 20-mg sample was placed in a tared platinum crucible (internal diameter: 6.5 mm, height: 4 mm). The sample then was heated from 50 to 1200–1250 °C at a heating rate of 10 °C min^{-1} under argon flowing at 50 mL min^{-1}. Isothermal TG measurements were carried out using a TA Instruments SDT Q600. An Alumina Calibration Weights Set manufactured by TA Instrument was used to calibrate the weight measurements of the TG. An ~ 20-mg sample was placed in tared alumina crucibles (internal diameter, 5.43 mm; height, 4 mm), ramp heated from room temperature to 300 °C at 10 °C min^{-1} and held at 300 °C for ~ 5 min to evaporate the moisture that might have been absorbed during storage. The sample was then ramp heated at 25 °C min^{-1} to each targeted temperature that ranged from 700 to 975 °C under ambient air flowing at 50 mL min^{-1}. The furnace temperature for both instruments was calibrated using the onset melt temperatures of high-purity metals (i.e., indium, tin, zinc, aluminum, and gold).

Results and discussion

Ramp heating

Figures 1 and 2 show the results of TG mass loss (red), differential TG (DTG) mass loss rate (blue), and DSC heat flow (black) as a function of temperature for pure alkali perrhenate salts of $NaReO_4$ (1a), $KReO_4$ (1b), and $CsReO_4$ (1c) and binary salts of $NaReO_4$-$KReO_4$ (2a), $NaReO_4$-$CsReO_4$ (2b), and $KReO_4$-$CsReO_4$ (2c). Table 1 summarizes the (1) measured melting points of three alkali

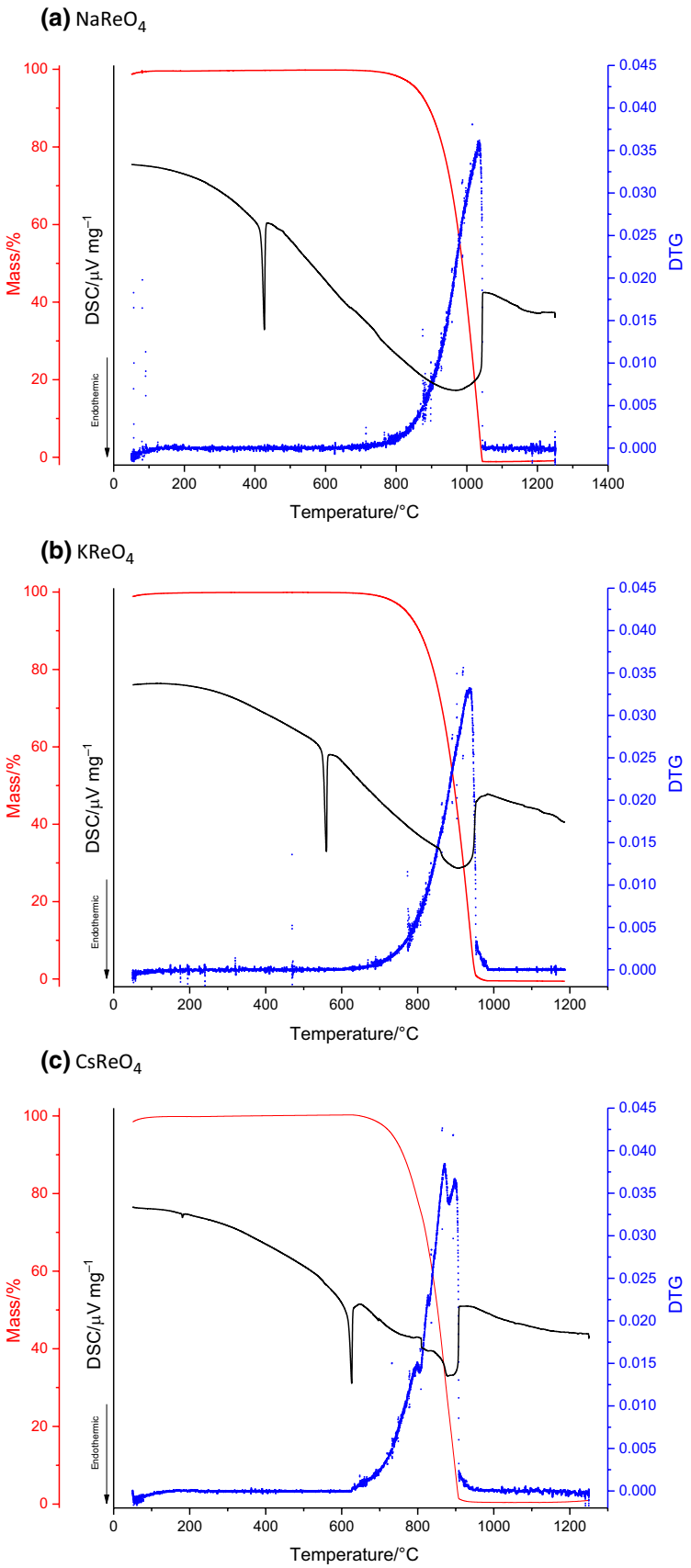

Fig. 1 TG (red), DTG (blue), and DSC (black) results of alkali perrhenates

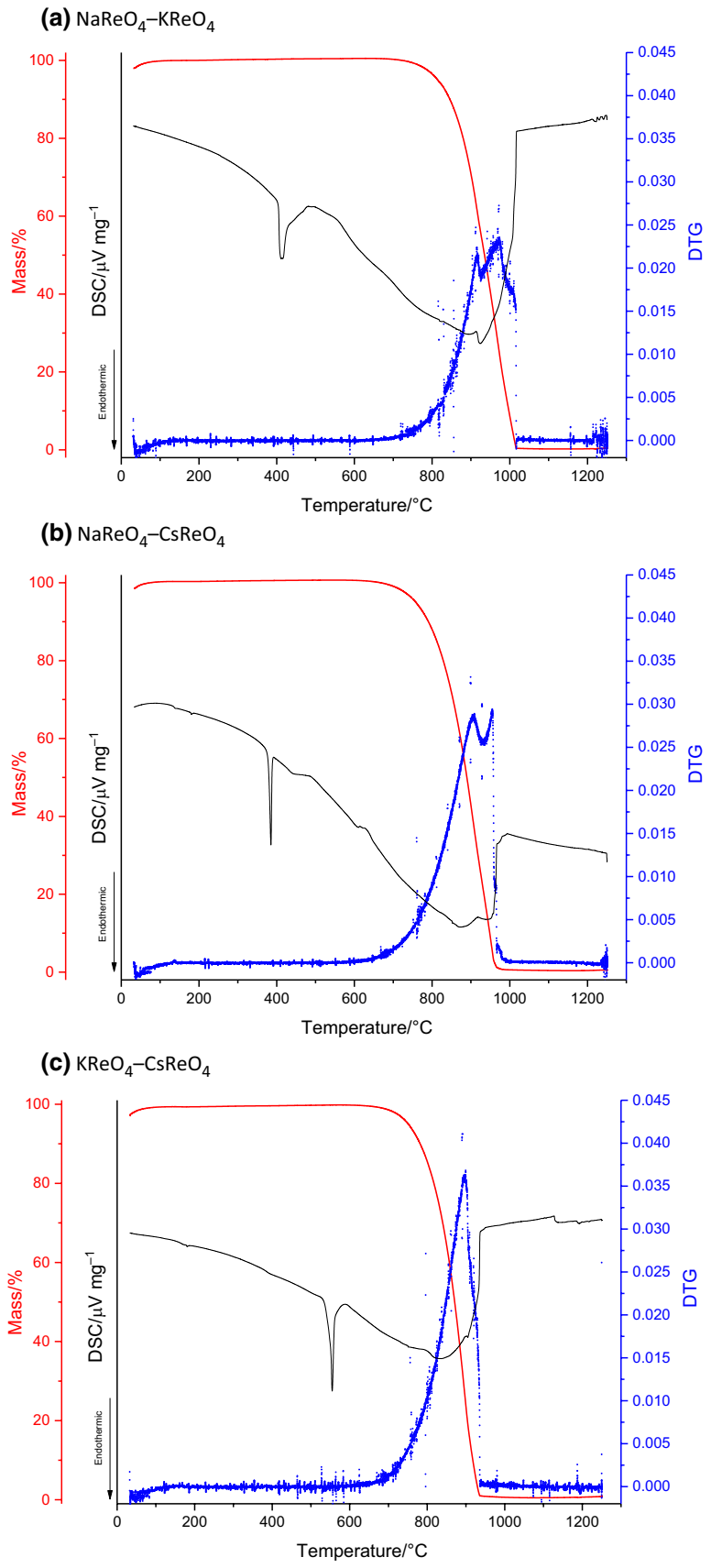

Fig. 2 TG, DTG and DSC results of binary alkali perrhenates mixtures

Table 1 Melting point and mass loss onset temperature of single and binary alkali perrhenate salts

Salt	Melting point, °C			Approximate mass loss onset temperature, °C
	This study	Smith [20]	Lukas [21]	
$NaReO_4$	420	414	420	720
$KReO_4$	555	555	555	660
$CsReO_4$	620	616	620	640
$NaReO_4$–$KReO_4$	415	NA	NA	660
$NaReO_4$–$CsReO_4$	385	NA	NA	625
$KReO_4$–$CsReO_4$	555	NA	NA	640

NA: not available

perrhenates determined by DSC compared with melting points reported in the literature [20, 21] and (2) mass loss onset temperature for all samples determined from DTG. The melting points show good agreement with published values for pure alkali perrhenates. Melting point data were not available in the literature for binary perrhenates.

As shown in Fig. 1a and Table 1, the melting point increases and approximate mass loss onset temperature (vaporization temperature) decreases as the atomic number of alkali metals increases. For $CsReO_4$ the melting point closely matches the vaporization temperature, suggesting that vaporization starts as soon as it melts. The melting point and vaporization temperature of binary salts should be equal to or lower than that of a salt with a lower melting point or vaporization temperature of the two salts. Table 1 shows that the melting points of $NaReO_4$-$KReO_4$ and $KReO_4$-$CsReO_4$ match that of $NaReO_4$ and $KReO_4$, respectively. However, the melting point of $NaReO_4$-$CsReO_4$ is considerably lower than that of $NaReO_4$, suggesting a eutectic type reaction between these two salts. The vaporization temperature of two binary salts—$NaReO_4$–$KReO_4$ and $KReO_4$–$CsReO_4$—agree well with that of a salt with the lower of two salts. However, the $NaReO_4$-$CsReO_4$ system had a slightly lower onset temperature than that of $CsReO_4$, which is likely related to the effect of the above-proposed eutectic formation in the $NaReO_4$-$CsReO_4$ system on the evaporation onset temperature. As shown in Fig. 2, the DSC peaks at the melting point of binary salts are sharp as with all single salts except $NaReO_4$–$KReO_4$ that showed a slightly widened peak, which may suggest a relatively slow melting of $KReO_4$ solid into liquid $NaReO_4$. Table 1 also shows that the vaporization temperature is always higher than 600 °C, which agrees with the observation that no noticeable volatilization of Re occurred below 600 °C during tests with two fully simulated Hanford LAW feeds [8, 22].

Figure 3 compares the TG curves of three single perrhenate salts and three mixed salts. The differences of estimated mass loss onset temperatures given in Table 1 are 60 °C for $NaReO_4$ vs. $KReO_4$ and 20 °C for $KReO_4$ vs. $CsReO_4$. However, as shown in Fig. 3, the temperature differences

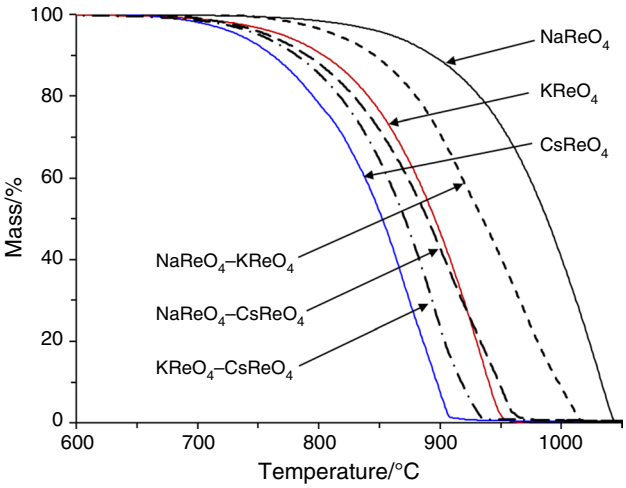

Fig. 3 Mass loss as a function of temperature for three single perrhenates and three mixed salts

increased with temperature reaching 90 and 45 °C, respectively, at ~ 90% mass% (10% evaporation), and these differences were roughly maintained until 100% evaporation. For these three salts, major volatility occurs at lower temperatures as atomic number increases although melting happens at higher temperatures.

Figure 3 also shows that the TG curves of mixed salts lie in between the corresponding curves of single salts, as expected, although not always midway between the two. To examine the correlation between the individual salts and their binary form for volatility, we used the following simple equation to calculate the mass loss curve expected if the individual salts in the binary mix behave independently without affecting each other:

$$f_b = f_1 w_1 + f_2(1 - w_1) \quad (1)$$

where f_b is the calculated mass loss fraction for the binary perrhenate salt, f_1 and f_2 are the mass loss fractions for the first and second perrhenate salts, respectively, determined by TG, and w_1 is the starting mass fraction of the first

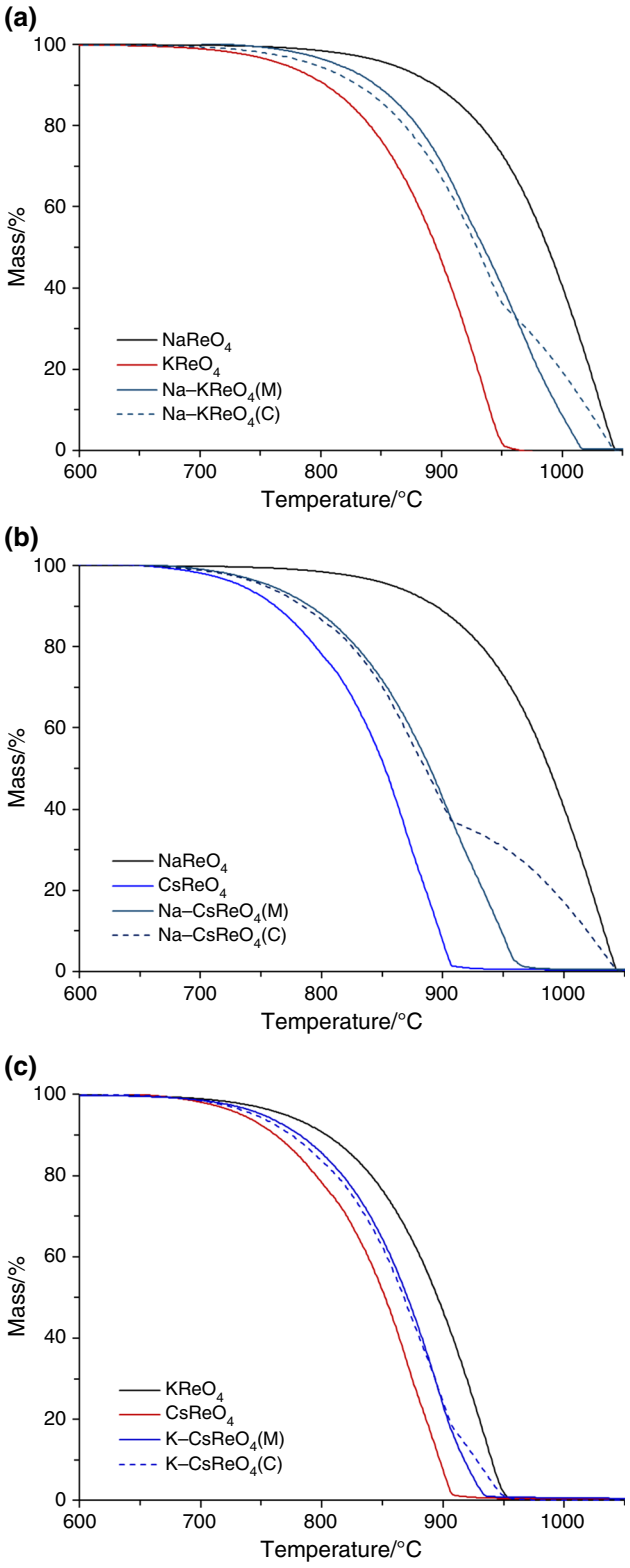

Fig. 4 Mass loss % as a function of temperature for three binary salt systems of (**a**) $NaReO_4$-$KReO_4$, (**b**) $NaReO_4$–$CsReO_4$, and (**c**) $KReO_4$–$CsReO_4$. Each plot includes TG curves for two single perrhenates, the measured binary curve (denoted by "M") and calculated curve (denoted by "C")

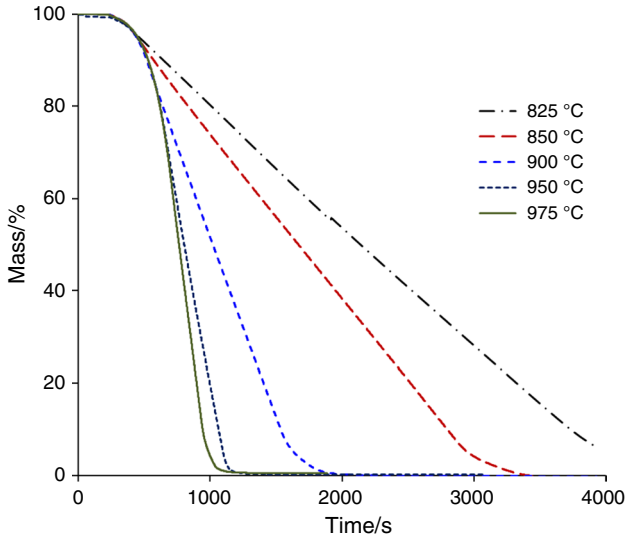

Fig. 5 Isothermal TG of $NaReO_4$

perrhenate salt in the binary perrhenate salt mix. Figure 4 shows overlaid TG curves of two single salts compared with that for their binary mixed salts for the three binary systems. For each plot in Fig. 4, the calculated mass loss fraction (dashed line) according to Eq. (1) is compared with those of measured for binary and single salts.

Figure 4 shows that the measured mass loss curves slightly fall behind or match the calculated curves until roughly the completion of mass loss for the single perrhenate that volatilizes at lower temperatures, for example, $KReO_4$ in the $NaReO_4$-$KReO_4$ system. In other words, the presence of less-volatile $NaReO_4$ may slow, although not significantly, the volatilization of more-volatile $KReO_4$. However, after this point, the measured curves deviate significantly from the calculated curves leading to accelerated mass loss of less-volatile $NaReO_4$ when compared to the volatilization of single $NaReO_4$, which suggests a potential interaction between the two perrhenates. As shown in Fig. 4, unlike the calculated mass loss curves of binary salts, the measured curves behave similarly to single salts without showing an inflection point, which may suggest the formation and volatilization of double perrhenate, for example, $NaK(ReO_4)_2$ in $NaReO_4$-$KReO_4$ system.

Isothermal heating

Figure 5 shows the results of isothermal TG for $NaReO_4$. As shown in the figure, the mass loss rate becomes linear after a short initial period when the rate accelerates and before tailing off toward the end of the test when only a small droplet is likely remaining. The other two alkali perrhenates also exhibited similar linear behavior (plots are not included). The linear periods of the test results were used to calculate

the $\frac{dm}{dt}$ using a surface area of 2.3×10^{-5} m^2 (5.43 mm ID). Table 2 summarizes the resulting mass loss data for the three alkali perrhenates.

We also performed isothermal TG runs for the three binary salts, and the results for the $NaReO_4$-$CsReO_4$ system as a function of temperature are shown in Fig. 6 as an example. The curves in the figure indicate that the salt mix does not volatilize monotonously as if one component, that is, the mass loss rate changes with time unlike single perrhenate salts shown in Fig. 5. This is likely because the composition of vaporizing salt changes with time as vaporization progresses. Figure 7 shows the results of isothermal TG at 825 °C for $NaReO_4$ and $CsReO_4$ and their binary mix. The binary salt behaves similarly to that observed from ramp heating tests shown in Fig. 4b. However, unfortunately, the apparent salt composition changes with time and the potential formation of double perrhenate precluded using them to estimate the vapor pressure of the alkali perrhenates discussed below.

Knudsen-cell effusion mass spectroscopy has been used in thermochemical studies of vaporization of some single and mixed perrhenates [11–18]. Price and coworkers [23, 24] showed that it is possible to use TG to measure vapor pressure of materials under ambient pressure conditions, using Eq. (2) adopted from the Langmuir equation [25] that relates the rate of free evaporation from the open surface to vapor pressure in a vacuum.

$$-\frac{dm_1}{dt} = P_1\alpha\sqrt{\frac{M_1}{2\pi RT}} \tag{2}$$

where $\frac{dm_1}{dt}$ is the rate of mass loss per unit area of vapor 1 (kg m^{-2} s^{-1}), P_1 is the vapor pressure of the vapor 1 (Pa), α is the vaporization coefficient, M_1 is the molecular mass of the vapor 1 (kg mol^{-1}), R is the gas constant (J mol^{-1} K^{-1}), and T is the temperature (K).

Table 2 Mass loss rate ($\frac{dm}{dt}$, kg m^{-2} s^{-1}) of alkali perrhenates from isothermal TG

Temperature/°C	$NaReO_4$	$KReO_4$	$CsReO_4$
700	NM	NM	2.29E-04
725	NM	NM	4.38E-04
750	NM	3.21E-04	6.62E-04
775	NM	4.72E-04	1.00E-03
800	NM	5.72E-04	1.37E-03
825	2.75E-04	9.42E-04	1.89E-03
850	3.93E-04	1.54E-03	2.64E-03
900	9.07E-04	2.13E-03	NM
950	1.71E-03	NM	NM
975	2.34E-03	NM	NM

NM not measured

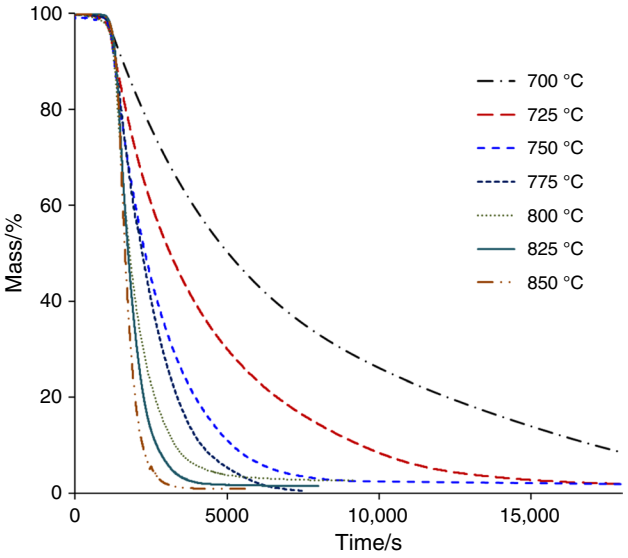

Fig. 6 Isothermal TG of $NaReO_4$–$Cs\ ReO_4$

However, Eq. (2) does not consider the kinetics of vapor diffusion through sample tube to the top where the vapor is swept away by a carrier gas [26–29]. The two major parameters that need to be considered include the diffusion coefficient and height of sample tube above the surface of molten sample (diffusion pass length). In the present study the initial sample height was approximately 5% of the total tube height and therefore the change of diffusion path length during evaporation is small and negligible.

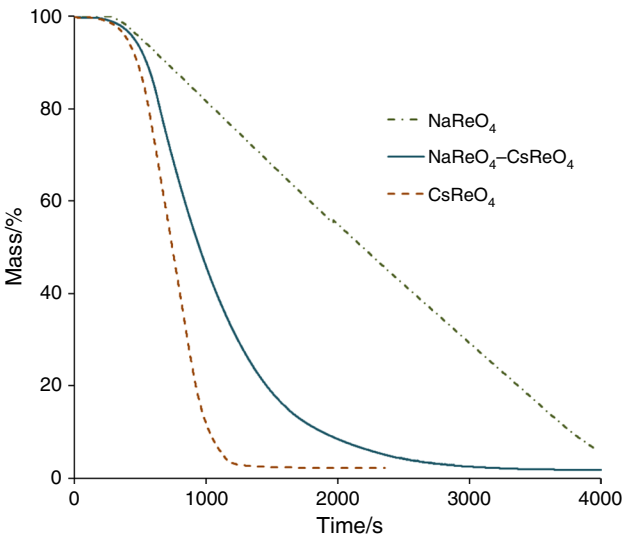

Fig. 7 Isothermal TG of $NaReO_4$, $NaReO_4$–$Cs\ ReO_4$, and $Cs\ ReO_4$ at 825 °C

Among the equations that describe the vaporization mass loss rate during diffusion-controlled evaporation [26–29], we adopted the equation derived by Pieterse and Focke [27]:

$$\frac{dm_1}{dt} = \left(\frac{M_1}{zRT}\right) P_1 D_{12} \tag{3}$$

where z is the diffusion path length (m) and D_{12} is the diffusion coefficient (m^2s^{-1}) of vapor 1 in vapor 2 (air in the present study). Equation (3) is chosen because the assumptions used to derive this equation were close to the conditions used in the present study. We also applied the equation for diffusion coefficient by Vlasov [29]:

$$D_{12} = \frac{C}{P_t \sigma_{12}^2 \Omega^*(T^*)} \sqrt{\frac{T^3}{2}\left(\frac{1}{M_1} + \frac{1}{M_2}\right)} \tag{4}$$

where C is a constant, P_t is the total pressure (atm), $\sigma_{12} = (\sigma_1 + \sigma_2)/2$ where σ_1 and σ_1 are the collision diameter of (nm) of vapors 1 and 2, and $\Omega^*(T^*)$ is the reduced collision integral that is calculated from the empirical equation for a given T^* [29]. The T^* is given as $T^* = kT/\varepsilon_{12}$ where $\varepsilon_{12} = \sqrt{\varepsilon_1 \varepsilon_2}$, ε_1/k and ε_2/k are the parameters of the Lennard–Jones potential for molecules of vapors 1 and 2, and k is a Boltzmann constant (J/K). The ε/k value for each vapor can be obtained from the relation $\varepsilon/k = 1.92T_m$, proposed by Wilke and Lee 1955 [30], where T_m is the melting point of each vapor specie (given in Table 1 for alkali perrhenates in this study and 58 K for air). Other researchers [31–33] proposed similar equations with differences in the constant C value (0.2628 for Vlasov 2020 [29]) and how the term $\Omega^*(T^*)$ is calculated.

Unfortunately, the data on σ_1 and σ_2 are not available for alkali perrhenates, therefore, it is not possible to directly calculate the vapor pressure from the mass loss data using Eqs. (3) and (4). Given the lack of information and considering that the primary interest in this study is the relative differences in the vapor pressure between the three alkali perrhenate, we used published vapor pressure data for $KReO_4$ by Lebedev 1962 [19], log[P, Torr] = 14,188/T + 13.282 (740–1000 °C), to fit the σ_{12} as a function of temperature. The fit results for the temperatures between 750 and 900 °C, where the mass loss was measured for $KReO_4$, were extrapolated to the temperatures the mass loss data are available for $NaReO_4$ and $CsReO_4$. It is noted that this exercise is valid only when the collision diameter (σ_1) is not grossly different between the three alkali perrhenates. Figure 8 shows the plots for the three salts with $KReO_4$ compared to that from Lebedev [19]. As shown in Fig. 8, the vapor pressure of perrhenate is in the order of $CsReO_4 > KReO_4 > NaReO_4$ for the temperature range of interest discussed in Jin et al. 2015 [22].

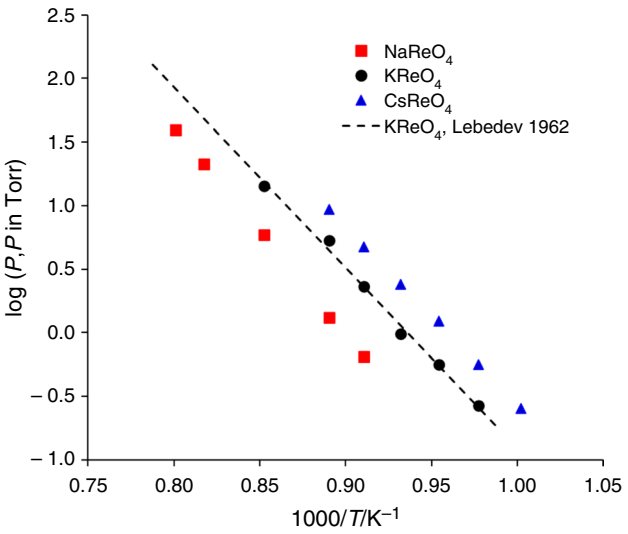

Fig. 8 Estimated vapor pressure of pure alkali perrhenates in this study compared with the measured for $KReO_4$ by Lebedev [19]

Summary and conclusions

Both the temperature ranges of evaporation determined by TG under ramp heating conditions and the vapor pressure estimated from isothermal TG support that the order of volatility of alkali perrhenates is $CsReO_4 > KReO_4 > NaReO_4$. This result agrees with the generally observed trend that the properties of alkali compounds follow the atomic number of alkali metals; that is, the unusual result observed from Hanford LAW glass feeds, the volatility order of $KReO_4 > CsReO_4 > NaReO_4$ discussed in Kim and Kruger [7], was not observed in the perrhenate salt systems used in our study. However, the volatility of the perrhenates is likely dependent on the composition of salt in which the perrhenates are dissolved. For Hanford LAW glass feeds, the primary salt that forms during early-stage melting is sodium nitrate/nitrite, although Jin et al. [22] proposed that the alkali perrhenate(s) are more preferentially associated with the minor sulfate-rich salt. We plan to investigate the effect of the solvent salt on the volatility of $KReO_4$ and $CsReO_4$ in a future study.

Supplementary Information The online version contains supplementary material available at https://doi.org/10.1007/s10973-021-11173-8.

Acknowledgements This research was supported by funding provided by the DOE's Waste Treatment and Immobilization Plant Project of the Office of River Protection. Pacific Northwest National Laboratory (PNNL) is operated for the DOE by Battelle Memorial Institute under Contract DE-AC05-76RL01830.

Author Contributions Pornsinee Cholsaipant performed isothermal TG tests, evaluated both isothermal and ramp heating TG data, and led overall manuscript writing. Jaime L George performed ramp heating

TG tests, evaluated the data, and contributed to writing ramp heating TG sections of the manuscript. Dongsang Kim was a principle investigator who primarily contributed to writing discussions and conclusions while supervising all test and data evaluation activities by Pornsinee Cholsaipant and Jaime George. Albert A Kruger provided technical guidance for the direction of the study and wrote portions of introduction section.

References

1. Gephart RE and Lundgren RE, Hanford tank clean up: A guide to understanding the technical issues, PNL-10773, Pacific Northwest National Laboratory, Richland, WA, 1995. Doi: https://doi.org/10.2172/195769.
2. Gephart RE. A short history of waste management at the Hanford Site. Phys Chem Earth Parts A/B/C. 2010;35(6–8):298–306. https://doi.org/10.1016/j.pce.2010.03.032.
3. River Protection Project System Plan, ORP-11242, Rev. 8 (2017), U.S. Department of Energy, Office of River Protection, Richland, WA 99352. https://www.hanford.gov/files.cfm/ORP-11242_System_Plan_Rev._8.pdf
4. Kim D. Glass property models, constraints, and formulation approaches for vitrification of high-level nuclear wastes at the us hanford site. J Korean Ceram Soc. 2015;52(2):92–102. https://doi.org/10.4191/kcers.2015.52.2.92.
5. Darab JG, Smith PA. Chemistry of technetium and rhenium species during low-level radioactive waste vitrification. Chem Mater. 1996;8(5):1004–21. https://doi.org/10.1021/cm950418.
6. McGrail BP, Bacon DH, Icenhower JP, Mann FM, Puigh RJ, Schaef HT, Mattigod SV. Near-field performance assessment for a low-activity waste glass disposal system: laboratory testing to modeling results. J Nucl Mater. 2001;298(1–2):95–111. https://doi.org/10.1016/S0022-3115(01)00576-1.
7. Kim D, Kruger AA. Volatile species of technetium and rhenium during waste vitrification. J Non-Cryst Solids. 2018;481:41–50. https://doi.org/10.1016/j.jnoncrysol.2017.10.013.
8. Jin T, Kim D, Tucker AE, Schweiger MJ, Kruger AA. Reactions during melting of low-activity waste glasses and their effects on the retention of rhenium as a surrogate for technetium-99. J Non-Cryst Solids. 2015;425:28–45.
9. Matlack KS, Muller IS, Pegg IL, and Joseph I, Improved technetium retention in Hanford LAW glass – phase 1, VSL-10R1920-1 (2010), Vitreous State Laboratory, The Catholic University of America, Washington, DC.
10. Matlack KS, Muller IS, Callow RA, D'Angelo N, Bardacki T, Joseph I, and Pegg IL, Improved technetium retention in Hanford LAW glass – phase 2, VSL-11R2260–1 (2011), Vitreous State Laboratory, The Catholic University of America, Washington, DC. https://www.osti.gov/servlets/purl/1458754
11. Rouschias G. Recent advances in the chemistry of rhenium. Chem Rev. 1974;74(5):531–66. https://doi.org/10.1021/cr60291a002.
12. Skudlarski K, Drowart J, Exsteen G, Vander Auwera-Mahieu A. Thermochemical study of vaporization of sodium and potassium perrhenate using a mass spectrometer. Trans Faraday Soc. 1967;63:1146–51. https://doi.org/10.1039/TF9676301146.
13. Skudlarski K, Lukas W. Mass spectrometric studies on the sublimation of rubidium perhhenate. J Less-Common Metals. 1973;31(3):329–35. https://doi.org/10.1016/0022-5088(73)90026-X.
14. Skudlarski K, Lukas W. Mass spectrometric studies on the vaporization of lithium perhhenate. J Less-Common Metals. 1973;33(1):171–6. https://doi.org/10.1016/0022-5088(73)90064-7.
15. Shugurov SM, Lopatin SI. Thermochemical study of gaseous salts of oxygen-containing acids: XXIV.1 polymers of alkali metals perrhenates. Rus J Gen Chem. 2008;78(10):1882–8. https://doi.org/10.1134/S1070363208100095.
16. Lukas W. The thermodynamic activity of $LiReO_4$ in the $LiReO_4$-$CsReO_4$ system as determined by mass spectrometry. J Less-Common Metals. 1979;66(2):211–7. https://doi.org/10.1016/0022-5088(79)90230-3.
17. Lukas W, Kowalska M, Skudlarski K. Mass Spectrometric determination of excess Gibbs free energy for (1–x)KReO4 + xCsReO4 at 806 K. J Chem Thermodyn. 1980;12(9):885–90. https://doi.org/10.1016/0021-9614(80)90034-8.
18. Lukas W. Thermodynamic properties of the $RbReO_4$-$CsReO_4$ System. Ber Bunsenges Phys Chem. 1988;92(5):600–3. https://doi.org/10.1002/bbpc.198800143.
19. Lebedev KB, The chemistry of rhenium, translated by L. Ronson, A.A. Woolfe, Butterworths, London, 1962.
20. Smith WT Jr, Long SH. The salts of Perrhenic Acid. I. The alkali metals and ammonium. J Am Chem Soc. 1948;70(1):354–6. https://doi.org/10.1021/ja01181a110.
21. Lukas W, Gaune-Escard M. Temperatures and enthalpies of melting of alkli-metal perrhenates. J Chem Thermodyn. 1982;14:593–7.
22. Jin T, Kim D, Kruger AA. Effects of sulfate on rhenium incorporation into low-activity waste glass. J Non-Cryst Solids. 2019;521:119528.
23. Price DM, Hawkins M. Calorimetry of two disperse dyes using thermogravimetry. Thermochim Acta. 1998;315(1):19–24. https://doi.org/10.1016/S0040-6031(98)00272-X.
24. Price DM. Vapor pressure determination by thermogravimetry. Thermochim Acta. 2001;367–368(8):253–62. https://doi.org/10.1016/S0040-6031(00)00676-6.
25. Langmuir I. The vapor pressure of metallic Tngsten. Phys Rev. 1913;2(5):329–42. https://doi.org/10.1103/PhysRev.2.329.
26. Beverley KJ, Clint JH, Fletcher PDI. Evaporation rates of pure liquids measured using a gravimetric technique. Phys Chem Chem Phys. 1999;1:149–53. https://doi.org/10.1039/A805344H.
27. Pieterse N, Focke WW. Diffusion controlled evaporation through a stagnant gas: estimating low vapour pressures from thermogravimetric data. Thermochim Acta. 2003;406(1–2):191–8. https://doi.org/10.1016/S0040-6031(03)00256-9.
28. Parker A, Babas R. Thermogravimetric measurement of evaporation: data analysis based on the Stefan tube. Thermochim Acta. 2014;595:67–73. https://doi.org/10.1016/j.tca.2014.09.011.
29. Vlasov VA. Diffusion-kinetic model of liquid evaporation from a Stefan tube: a solution to the Stefan diffusion problem. Int J Heat Mass Transf. 2020;163: 120379. https://doi.org/10.1016/j.ijheatmasstransfer.2020.120379.
30. Wilke CR, Lee CY. Estimation of diffusion coefficients for gases and vapors. Ind Eng Chem. 1955;47(6):1253–7. https://doi.org/10.1021/ie50546a056.
31. Gilliland ER. Diffusion coefficients in gaseouse systems. Ind Eng Chem. 1934;26(6):681–5. https://doi.org/10.1021/ie50294a020.
32. Fuller EN, Schettler PD, Giddings JC. A new method for prediction of binary gas-phase diffusion coefficeitns. Ind Eng Chem. 1966;58(5):18–27. https://doi.org/10.1021/ie50677a007.
33. Holsen JN, Strunk MR. Binary diffusion coefficients in nonpolar gases. Ind Eng Chem Fundam. 1964;3(2):143–6. https://doi.org/10.1021/i160010a010.